2013 IEEE/RSJ International Conference on
Intelligent Robots and Systems (IROS)
September 14-18, 2014. Chicago, IL, USA,

Magnetic-Based Motion Control of Sperm-Shaped Microrobots using Weak Oscillating Magnetic Fields

Islam S. M. Khalil*, Kareem Youakim*, Alonso Sánchez†, and Sarthak Misra†

***Abstract*— We experimentally demonstrate that using oscillating weak magnetic fields a sperm-shaped microrobot (which we refer to as MagnetoSperm) can swim using flagellar propulsion and slide on a surface under water. The sperm morphology allows the MagnetoSperm to mimic the locomotion mechanism of a living sperm cell. The MagnetoSperm is designed and developed with a magnetic head and a flexible tail to provide a magnetic dipole moment and propulsion, respectively. The head oscillates under the influence of controlled oscillating weak magnetic fields (∼5 mT). This oscillation generates a thrust force in the flexible tail, and hence allows the MagnetoSperm to overcome the drag and friction forces during swimming and sliding on a surface, respectively. Point-to-point open- and closed-loop control of the MagnetoSperm are accomplished using an electromagnetic system under microscopic guidance. This motion control is done in two cases, i.e., swimming in water and sliding on a surface. At oscillating magnetic field of 5 Hz and 45 Hz, the MagnetoSperm swims at an average swimming speed of 32 μm/s (0.1 body lengths per second) and 158 μm/s (0.5 body lengths per second), respectively. At the same frequencies, the MagnetoSperm slides on the bottom of a petri-dish at an average speed of 21 μm/s (0.07 body lengths per second) and 6 μm/s (0.02 body lengths per second), respectively.**

I. INTRODUCTION

Microrobots have the potential to achieve non-trivial tasks such as minimally invasive surgeries and selectively deliver drugs to diseased cells [1], [2]. Therefore, much effort has been made to find the optimal methods for propulsion [5]-[13]. One propulsion method is to pull magnetic microrobots using the magnetic field gradient [14]-[16]. However, the projection distance of the magnetic field gradient is less than that of the magnetic field [1]. This property decreases the usefulness of pulling magnetic microrobots using the field gradient since its not reasonable to scale-up electromagnetic systems (with closed-configurations). Self-driven microrobots [3], [4] benefit from the relatively larger projection distance of the magnetic field that is used only for steering.

A helical microrobot is moved using a rotating magnetic field by helical propulsion. The dipole moment of the microrobot continuously aligns itself with the rotating magnetic field [17]-[20]. The magnetic torque then rotates the microrobot resulting in its forward propulsion. Similar to the previous helical propulsion, research has also been done on microrobots based on flagellar propulsion. These microrobots consist of artificial magnetic flagellum. The flagellum is synthesized using magnetic microparticles (with diameter of 1 μm) connected together by short flexible joints. The microrobots oscillate when an oscillating magnetic field is applied [13]. An additional technique to create an artificial flagellum is to glue rectangular coils (with length and width of 7 mm and 5 mm, respectively) together. Input currents of opposite directions are applied to these coils to generate magnetic moments when a uniform magnetic field is applied [21]. These magnetic moments generate a traveling wave along the coils resulting in a thrust force. Ye *et al.* have designed submillimeter-scale robot with multiple flagella and showed that its swimming speed increases linearly with the number of flagella [22].

In this study, we develop a sperm-shaped microrobot which we refer to as MagnetoSperm [6]. The propulsion of the MagnetoSperm is accomplished using oscillating weak magnetic fields that are generated using an orthogonal array

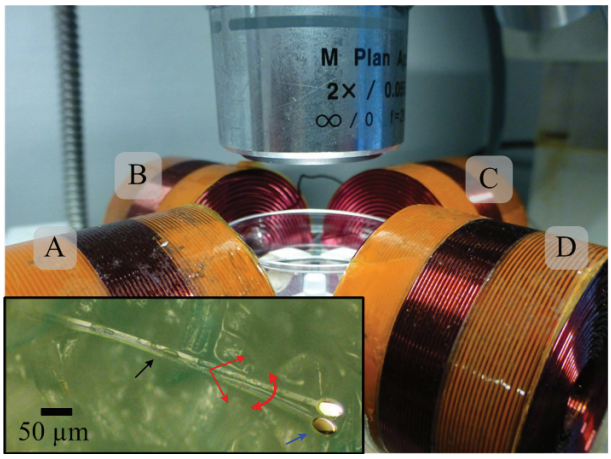

Fig. 1. An electromagnetic system [8] for the wireless magnetic-based control of MagnetoSperm (inset) [6]. MagnetoSperm consists of a magnetic head and a flexible structure that provide magnetic dipole moment and propulsion, respectively. MagnetoSperm is contained inside a petri-dish. The magnetic system generates weak (∼5 mT) oscillating magnetic fields (red arrows) to propel MagnetoSperm. Propulsion is achieved by exerting a magnetic torque on the magnetic head of MagnetoSperm (blue arrow) to oscillate the flexible tail (black arrow). Using the oscillating weak magnetic fields, MagnetoSperm can swim and slide on a surface. The letters A, B, C, and D indicate the electromagnetic coils.

This work was supported by funds from MIRA–Institute for Biomedical Technology and Technical Medicine, University of Twente, The Netherlands

*Islam S. M. Khalil and Kareem Youakim are affiliated with the Faculty of Engineering and Material Science (EMS), the German University in Cairo, New Cairo City, Egypt islam.shoukry@guc.edu.eg

†Alonso Sánchez and Sarthak Misra are affiliated with MIRA–Institute for Biomedical Technology and Technical Medicine (Robotics and Mechatronics Group), University of Twente, Enschede, The Netherlands s.smisra@utwente.nl

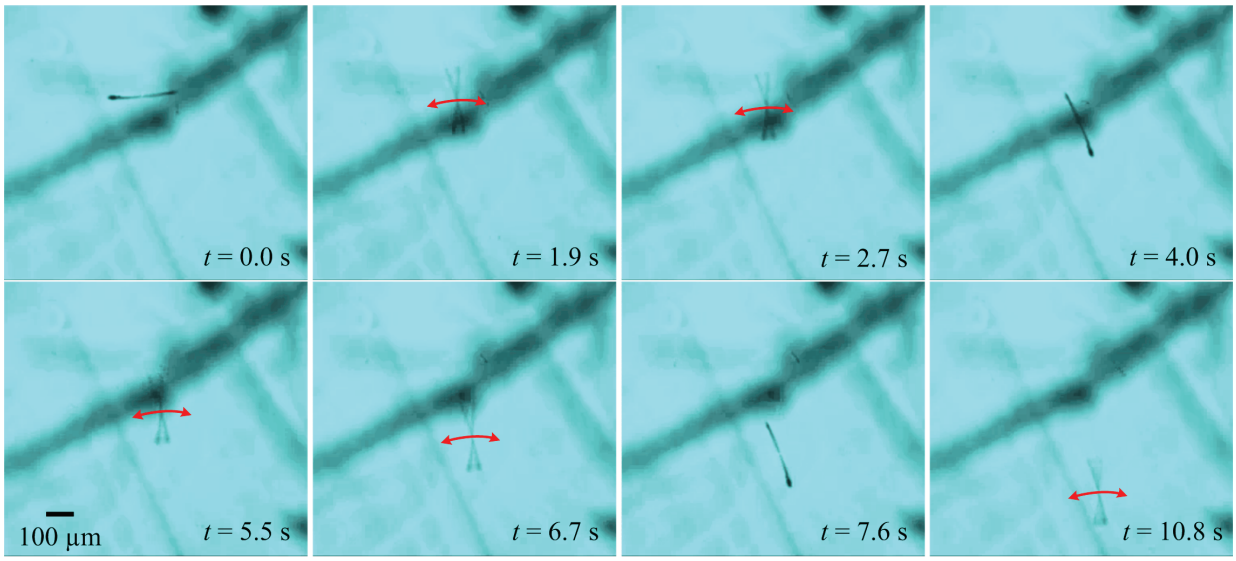

Fig. 2. A representative open-loop motion control of MagnetoSperm using oscillating weak magnetic fields when MagnetoSperm is immersed in water without contact with the bottom of the petri-dish. These fields are switched on at times, $t = 1.9$ seconds and $t = 5.5$ seconds, and off, at times $t = 4.0$ seconds and $t = 7.6$ seconds to experimentally demonstrate that MagnetoSperm is driven under the influence of the applied oscillating weak magnetic fields. The swimming speed in this open-loop experiment is 107 μm/s for oscillating magnetic field at frequency of 50 Hz. *Please refer to the accompanying video that demonstrates the open-loop control result of MagnetoSperm.*

of electromagnetic coils (Fig. 1). We design a closed-loop control system that allows us to generate oscillating fields that points towards a reference position. This control strategy allows the MagnetoSperm to be oriented and swim towards the reference position. Furthermore, we experimentally demonstrate that the oscillating weak magnetic fields allow the MagnetoSperm to move when in contact with a surface (bottom of the petri-dish).

The remainder of this paper is organized as follows: Section II provides descriptions pertaining to the manufacturing and modeling of the MagnetoSperm. Section III describes our closed-loop motion control strategy based on microscopic guidance. Point-to-point motion control results of the MagnetoSperm are included in Section IV. This control is implemented when the MagnetoSperm is swimming in water and sliding on a surface under water. Finally, Section V concludes and provides directions for future work.

II. DEVELOPMENT AND MODELING OF THE MAGNETOSPERM

MagnetoSperm consists of a magnetic head with a cobalt-nickel layer ($Co_{80}Ni_{20}$) and a flexible tail, as shown in Fig. 2. Applying an oscillating magnetic fields exerts a magnetic torque on the magnetic dipole moment of MagnetoSperm. This torque oscillates the flexible tail and results in a thrust force that overcomes the drag force while swimming and friction force while sliding on a surface. In this Section, we describe the fabrication steps of MagnetoSperm and its linear and rotational dynamics.

A. Fabrication of The MagnetoSperm

Fabrication of the MagnetoSperm is done using two steps [6]. First, development of the main body (head, neck and tail). Second, deposition of the magnetic material on the head. SU-8 is selected as the structural material for the main body due to its mechanical stability and ease of fabrication. A silicon wafer with $< 100 >$ crystal orientation is initially spin coated with SU-8-5. The thickness and the diameter of this wafer are 500 μm and 100 mm, respectively. Following the pre-bake of the wafer, the MagnetoSperm patterns are transferred to the SU-8 layer by ultraviolet (UV) exposure. The wafer is further baked (post-exposure bake) and the MagnetoSperm bodies are realized by developing the SU-8 layer in RER600 (ARCH Chemicals, Basel, Switzerland). The mechanical stability is achieved by hard baking the wafer. The magnetic material on the head of the MagnetoSperm is developed through a lift-off procedure. The layout of the magnetic material is transferred onto the MagnetoSperm by spin-coating the wafer a 10 μm-thick photoresist (AZ 9260) and UV-exposure. After 30 seconds of oxygen plasma treatment, to enhance the adhesion of the metal layer to the SU-8, a 200 nm-thick cobalt-nickel layer is deposited by e-beam evaporation and lifted-off in acetone. Oxygen plasma treatment is then performed on the MagnetoSperm for 30 seconds to make the SU-8 hydrophilic. Finally, the MagnetoSperm is released by etching away the silicon wafer in a 5% TMAH solution at 85°C and the solution is diluted. After the development of MagnetoSperm, a magnetic system with an orthogonal array of electromagnetic coils is used to control its motion.

B. Modeling of The MagnetoSperm

Under the influence of a magnetic field, the magnetic force $\left(\mathbf{F}\left(\mathbf{P}\right) \in \mathbb{R}^{3\times1}\right)$ and torque $\left(\mathbf{T}\left(\mathbf{P}\right) \in \mathbb{R}^{3\times1}\right)$ experienced by the magnetic head of MagnetoSperm located at position

$\left(\mathbf{P} \in \mathbb{R}^{3\times1}\right)$ are given by [23], [24]

$$\mathbf{F}(\mathbf{P}) = (\mathbf{m}\cdot\nabla)\mathbf{B}(\mathbf{P}) \quad \text{and} \quad \mathbf{T}(\mathbf{P}) = \mathbf{m}\times\mathbf{B}(\mathbf{P}), \tag{1}$$

where $\mathbf{m} \in \mathbb{R}^{3\times1}$ and $\mathbf{B}(\mathbf{P}) \in \mathbb{R}^{3\times1}$ are the magnetic dipole moment of MagnetoSperm and the induced magnetic field, respectively. A lower limit of the drag force on MagnetoSperm can be obtained by neglecting its head and assuming that its morphology is similar to a long thin needle of length l and diameter d [25]:

$$\mathbf{F_d}(\dot{\mathbf{P}}) = \eta\frac{l}{\ln(\frac{2l}{d}) - 0.81}\dot{\mathbf{P}}, \tag{2}$$

where $\mathbf{F_d}(\dot{\mathbf{P}}) \in \mathbb{R}^{3\times1}$ and $\dot{\mathbf{P}} \in \mathbb{R}^{3\times1}$ are the drag force and the velocity of MagnetoSperm, respectively. Further, η is the dynamic viscosity of water (1 mPa.s), and l and d are the length (322 μm) and diameter (5.2 μm) of MagnetoSperm, respectively. Using (2), the linear drag force is calculated to be 1.2×10^{-11} N at a speed of 158 μm/s (maximum average speed of MagnetoSperm at frequency of 45 Hz). Using (1), the magnetic force exerted on the magnetic dipole of MagnetoSperm is given by

$$\mathbf{F}(\mathbf{P}) = \int_v M_s \mathrm{d}v\cdot\nabla\mathbf{B}(\mathbf{P}) = \mathbf{m}\cdot\nabla\mathbf{B}(\mathbf{P}), \tag{3}$$

where $\mathbf{F}(\mathbf{P})$ is the magnetic force at point $(\mathbf{P})$. Further, M_s and v are the magnetization saturation (1.19×10^6 A/m) and volume of the $Co_{80}Ni_{20}$ that is deposited on the head of the MagnetoSperm, respectively. Using (3), the maximum magnetic force exerted on the MagnetoSperm is calculated to be 3.89×10^{-13} N at magnetic field gradient of 2 mT/m. This calculation shows that the maximum magnetic force exerted on MagnetoSperm by our magnetic system is 2 orders-of-magnitude smaller than the drag force. Therefore, motion of MagnetoSperm (Fig. 2) is mainly due to the thrust force generated based on the oscillation of the flexible tail. This result would allow us to steer and propel the MagnetoSperm using weak magnetic fields without the magnetic field gradients.

For *in vivo* applications, contact could occur between the MagnetoSperm and a surface (blood vessel or tissue). Therefore, equation of motion of the MagnetoSperm is given by

$$\mathbf{F}(\mathbf{P}) + \mathbf{F_d}(\dot{\mathbf{P}}) + \mathbf{F_t} + \mu_s\mathbf{R} = 0, \tag{4}$$

where $\mathbf{F_t}$ is the propulsion force generated by the flexible tail due to the oscillating magnetic fields. Further, μ_s and $\mathbf{R}$ are the static coefficient of friction between the MagnetoSperm and a surface, and the reaction force on the MagnetoSperm, respectively. The rotational dynamics of the MagnetoSperm is given by

$$|\mathbf{B}(\mathbf{P})||\mathbf{m}|\sin(\beta) + \alpha\dot{\theta} + \mu_s\mathbf{R}l = 0, \tag{5}$$

where β is the angle between the induced magnetic field and the magnetic dipole moment of the MagnetoSperm. Further, $\dot{\theta}$ and α are the angular velocity of the MagnetoSperm and the rotational drag coefficient, respectively.

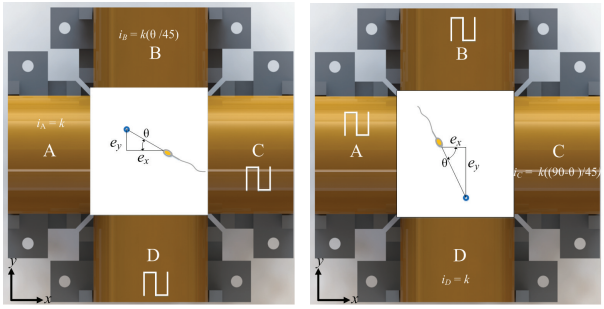

(a) MagnetoSperm swims towards a reference position (b) MagnetoSperm swims towards a reference position

Fig. 3. Schematic representation of the control strategy used to allow the MagnetoSperm to swim or slide on a surface towards the reference position (small blue circle). The angle of the MagnetoSperm with respect to x-axis is indicated by θ. Further, e_x and e_y represent the position tracking errors along x- and y-axis, respectively. The letters A, B, C, and D indicate the electromagnetic coils. The currents at electromagnets A, B, C, and D are indicated by i_A, i_B, i_C, and i_D, respectively. (a) MagnetoSperm is oriented towards the top left quadrant by electromagnets A and B. Electromagnets C and D provide oscillating fields to oscillate the magnetic head of MagentoSperm. (b) Electromagnets C and D provide uniform magnetic fields in the direction of the reference point. Electromagnets A and B generate oscillating magnetic fields.

In (4), the magnetic force (**F(P)**) does not allow for pulling the MagnetoSperm towards the reference. However, it contributes to the propulsion force generated by the oscillating tail in overcoming the drag force and the friction force (when the MagnetoSperm is in contact with a surface). The rotational dynamics (5), indicates that the magnetic torque must overcome the rotational drag and the frictional torque. Therefore, the angle (β) between the magnetic fields $(\mathbf{B}(\mathbf{P}))$ and the magnetic dipole moment $(\mathbf{m})$ has to be 90° to maximize the magnetic torque exerted on the magnetic dipole of the MagnetoSperm.

III. MOTION CONTROL DESIGN

Four electromagnetic coils are used to control the motion of the MagnetoSperm along x- and y-axis. Two electromagnets are supplied with square current inputs to oscillate the magnetic head of the MagnetoSperm. The other two electromagnets control the orientation of the MagnetoSperm. We calculate the position tracking errors between the magnetic head and the reference position using:

$$e_x = x_{\text{ref}} - x \quad \text{and} \quad e_y = y_{\text{ref}} - y, \tag{6}$$

where e_x and e_y are the position tracking errors along x- and y-axis, respectively. Further, x_{ref} and y_{ref} are the components of the fixed reference position (Fig. 3), and x and y are the position of the magnetic head of the MagnetoSperm (indicated using the large blue circle in Fig. 4). The orientation angle of the MagnetoSperm (θ) is given by

$$\theta = \tan^{-1}\left(\frac{|e_x|}{|e_y|}\right). \tag{7}$$

Each electromagnet either produces an oscillating field or a uniform field (within the center of the workspace). The

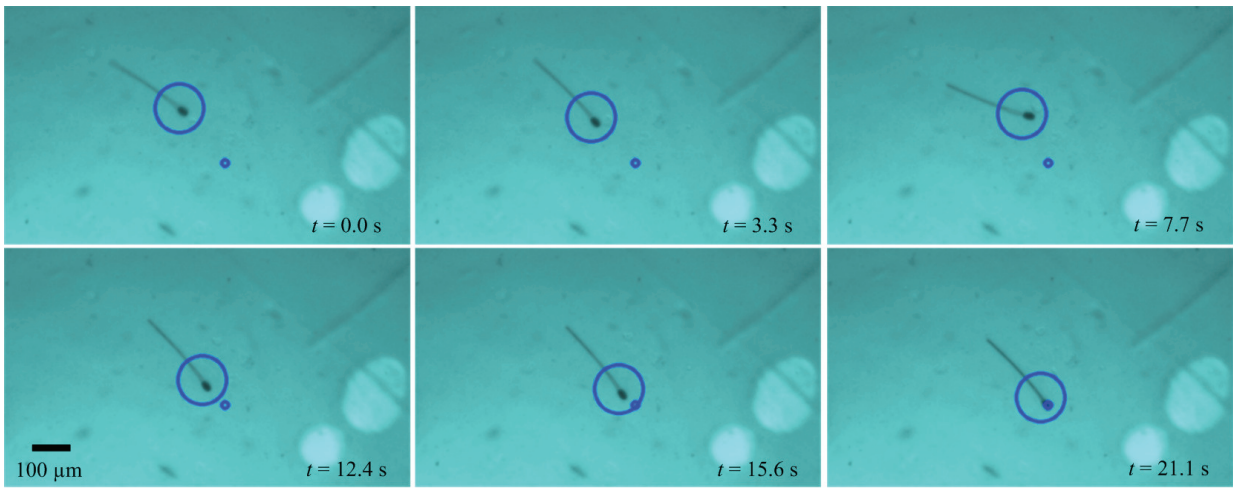

Fig. 4. A representative closed-loop motion control of the MagnetoSperm when in contact with the bottom of the petri-dish. MagnetoSperm slides on the bottom of the petri-dish towards the reference position (small blue circle) at a sliding speed of 12 μm/s, at an oscillating magnetic field with frequency of 5 Hz. The large blue circle is assigned using our feature tracking algorithm [8], and it indicates the head of the MagnetoSperm. *Please refer to the accompanying video that demonstrates the closed-loop control result of the MagnetoSperm.*

electromagnets producing the oscillating fields are always in the opposite direction to the direction of movement of the MagnetoSperm. The other two electromagnets provide uniform magnetic fields towards the reference position. The electromagnets that generate uniform magnetic fields are determined based on the position of the reference (small blue circle) and the MagnetoSperm. Then the current magnitude at each of these electromagnets is calculated to adjust the direction of the MagnetoSperm. When θ is $45°$, both electromagnets are supplied with the same current input, i.e., k. As θ increases or decreases, the current input on one electromagnet must be decreased to allow the other electromagnet to orient the MagnetoSperm towards its direction. The current supplied is a ratio between θ and $45°$ multiplied by k. Fig. 3(a) shows an example of the MagnetoSperm moving towards a reference point, and θ is less than $45°$. Electromagnet D and C generate oscillating fields. Electromagnet A is supplied with k while electromagnet B is supplied with a current input of $k\frac{\theta}{45}$. In order to keep the ratio less than 1 when θ is more than $45°$, the current supply becomes $k\frac{90-\theta}{45}$ A as in the case shown in Fig. 3(b).

IV. EXPERIMENTAL RESULTS

Our motion control strategy is based on orienting the MagnetoSperm towards a reference position, then oscillating the magnetic fields to allow for its swimming or sliding towards the reference.

A. Open-Loop Control

Open-loop motion control of the MagnetoSperm is done by using two opposite electromagnets to generate uniform magnetic fields (within the center of the workspace of our magnetic system), and using the other opposite electromagnets to oscillate these fields. Fig. 2 shows a representative open-loop motion control result of the MagnetoSperm. At time $t = 0$ seconds, zero magnetic fields are applied using the electromagnetic coils and the MagnetoSperm is oriented towards coil A (Fig. 1). At time $t = 1.9$ seconds, uniform magnetic fields are applied using electromagnets B and D, and sinusoidal currents are applied to electromagnets A and C to oscillate the uniform magnetic fields. The angle between the oscillating magnetic field lines is approximately $90°$. This angle is determined by simulating the oscillating magnetic fields using a verified finite element model [28]. The FE model is created using Comsol Multiphysics® (COMSOL, Inc., Burlington, U.S.A). As shown in Fig. 2, the MagnetoSperm swims under the influence of the oscillating magnetic fields. At time $t = 4.0$ seconds, the oscillating magnetic fields are only switched off and the MagnetoSperm stops swimming. At time $t = 5.5$ seconds, the oscillating magnetic fields are switched on again and the MagnetoSperm swims along the oscillating magnetic field lines, and so forth. We observe that the MagnetoSperm swims at a speed of 107 μm/s at a frequency of 50 Hz. This open-loop experiment is repeated 5 times and the average swimming speed at 50 Hz is calculated to be 125 μm/s. *Please refer to the accompanying video that demonstrates the flagellated swim and the open-loop control of the MagnetoSperm.*

B. Closed-Loop Control

The position of the MagnetoSperm is determined using a feature tracking algorithm, and used to calculate the position tracking errors along x- and y-axis. These errors are used to compute the angle (θ) of the MagnetoSperm using (7). Currents at each of the electromagnets are calculated based on this angle. Fig. 4 shows a representative closed-loop control of the MagnetoSperm. In this experiment, the MagnetoSperm is in contact with the bottom of the petri-dish and is subjected to friction and drag forces based on (4). Based on the control strategy (Section III), electromagnets A and B

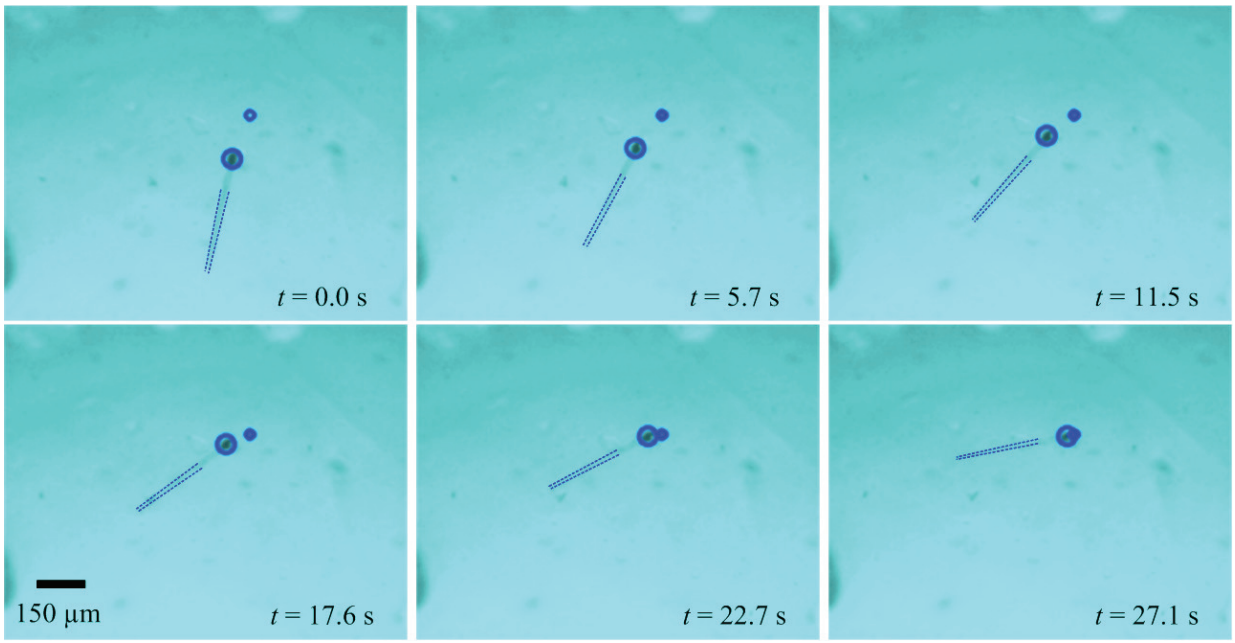

Fig. 5. A representative closed-loop motion control of the MagnetoSperm when in contact with the bottom of the petri-dish. The MagnetoSperm slides towards the reference position (small blue circle) at a sliding speed of 5 μm/s, at an oscillating magnetic field with frequency of 45 Hz. The large blue circle is assigned using our feature tracking algorithm [8], and it indicates the head of the MagnetoSperm. The dashed-blue lines indicate the flexible tail of MagnetoSperm. *Please refer to the accompanying video that demonstrates the closed-loop control result of the MagnetoSperm.*

generate oscillating magnetic fields, whereas electromagnets C and D generate uniform magnetic fields towards the reference position (the small blue circle). As shown in Fig. 4, the MagnetoSperm slides towards the reference position and is localized within its vicinity at a speed of 12 μm/s. Fig. 5 shows another representative closed-loop control of the MagnetoSperm at oscillating magnetic field of 45 Hz. Based on the position of the magnetic head and the given reference position, electromagnets B and C generate uniform magnetic fields towards the reference position, whereas electromagnets A and D oscillate these fields to move the MagnetoSperm towards the reference position. The sliding speed of the MagnetoSperm in this experiment is 5 μm/s. The frequency of the oscillating magnetic fields is 5 Hz. *Please refer to the accompanying video that demonstrates the closed-loop control of the MagnetoSperm.*

We repeat the closed-loop motion control of the MagnetoSperm 5 times at 2 frequencies of the oscillating magnetic fields, i.e., 5 Hz and 45 Hz. These experiments are done when the MagnetoSperm is in contact with the bottom of the petri-dish. The average position tracking errors are calculated to be 33 μm and 20 μm at frequencies of 5 Hz and 45 Hz for the oscillating magnetic field, respectively. The average sliding speeds are calculated to be 21 μm/s and 6 μm/s at frequencies of 5 Hz and 45 Hz for the oscillating magnetic field, respectively. This indicates that the speed of the MagnetoSperm is inversely proportional to the frequency of the oscillating magnetic fields, as shown in Fig. 6 . Furthermore, we observe that the swimming speed of the MagnetoSperm (no contact with the bottom of the petri-dish) increases as we increase the frequency of the oscillating magnetic fields. At frequency of 5 Hz and 45 Hz, the swimming speeds are calculated to be 30 μm/s and 158 μm/s, respectively. This observation suggests that the frequency of the oscillating weak magnetic field should be devised based on the position of the MagnetoSperm with respect to a surrounding surface such as a blood vessel, tissue, and walls of the arterial networks. A higher frequency can be devised when the MagnetoSperm is swimming, and once it contacts a surface and start sliding the frequency of the oscillating field has to be decreased.

V. CONCLUSIONS AND FUTURE WORK

We design a sperm-shaped microrobot and analyze its motion control characteristics when immersed in water and in contact with a surface. Our experimental results show that the swimming speed increases (0.1 body length per seconds and 0.5 body length per seconds at 5 Hz and 45 Hz, respectively) as we increase the frequency of the oscillating magnetic fields. Moreover, we show that the sliding speed decreases (0.07 body lengths per second and 0.02 body lengths per second at 5 Hz and 45 Hz, respectively) as we increase the frequency of the oscillating magnetic fields.

As part of future work, the MagnetoSperm will be controlled in the three dimensional-space (3D) [26], and its frequency response will be characterized. This characterization will be done when the MagnetoSperm is swimming and sliding on a surface under water. Furthermore, its parameters (stiffness of the tail and shape of the head) will be optimized to provide maximum propulsion force during

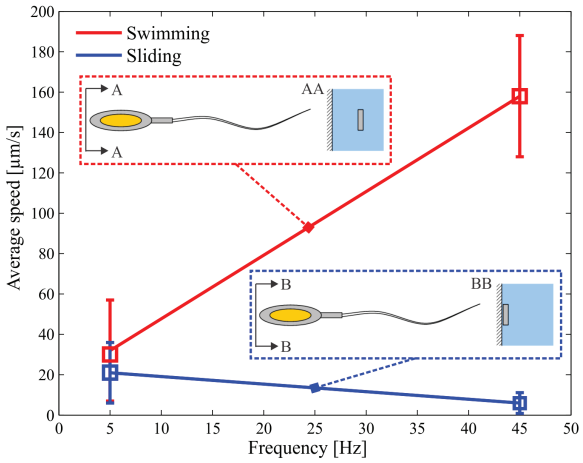

Fig. 6. Swimming and sliding speeds of the MagnetoSperm at two representative frequencies of the oscillating weak magnetic fields, i.e., 5 Hz and 45 Hz. The swimming and sliding speeds of MagnetoSperm are calculated based on 5 open-loop control trails at each frequency. The swimming and sliding experiments are done while MagnetoSperm is immersed in water and in contact with the bottom of a petri-dish, respectively.

flagellated swim. An ultrasound imaging modality [27] will be incorporated to the control system to accomplish closed-loop control of MagnetoSperm in 3D space.

VI. Acknowledgment

The authors thank Mr. Herman C. Dijkslag for collecting the data used in Fig. 2. They would also like to thank Ms. Ozlem Sardan Sukas for assistance with the design and manufacturing of the MagnetoSperm.

References

[1] B. J. Nelson, I. K. Kaliakatsos, and J. J. Abbott, "Microrobots for minimally invasive medicine," *Annual Review of Biomedical Engineering*, vol. 12, pp. 55-85, April 2010.

[2] J. Wang and W. Gao, "Nano/Microscale Motors: Biomedical Opportunities and Challenges," *ACS Nano*, vol. 6, no. 7, pp. 5745-5751, July 2012.

[3] S. Martel, C. C. Tremblay, S. Ngakeng, and G. Langlois, "Controlled manipulation and actuation of micro-objects with magnetotactic bacteria," *Applied Physics Letters*, vol. 89, no. 23, pp. 1-3, 2006.

[4] M. S. Sakar, E. B. Steager, D. H. Kim, A. A. Julius, M. Kim, V. Kumar, and G. J. Pappas, "Modeling, control and experimental characterization of microbiorobots," *International Journal of Robotics Research*, vol. 30, no. 6, pp. 647-658, May 2011.

[5] J. J. Abbott, K. E. Peyer, L. Dong, and B. Nelson, "How should Microrobots Swim?, "*The International Journal of Robotics Research*, vol. 28, no. 11-12, pp. 1434-1447, November 2009.

[6] I. S. M. Khalil, H. C. Dijkslag, L. Abelmann, and S. Misra, "MagnetoSperm: A microrobot that navigates using weak magnetic fields," *Applied Physics Letters*, 104, 223701, June 2014.

[7] I. S. M. Khalil, M. P. Pichel, L. Abelmann, and S. Misra, "Closed-loop control of magnetotactic bacteria," *The International Journal of Robotics Research*, vol. 32, no. 6, pp. 637-649, May 2013.

[8] I. S. M. Khalil, J. D. Keuning, L. Abelmann, and S. Misra, "Wireless magnetic-based control of paramagnetic microparticles," in *Proceedings of the IEEE RAS/EMBS International Conference on Biomedical Robotics and Biomechatronics (BioRob)*, pp. 460-466, Rome, Italy, June 2012.

[9] A. A. Solovev, Y. F. Mei, E. B. Urena, G. Huang, and O. G. Schmidt, "Catalytic microtubular jet engines self-propelled by accumulated gas bubbles," *Small*, vol. 5, no. 14, pp. 1688-1692, July 2009.

[10] W. F. Paxton, K. C. Kistler, C. C. Olmeda, A. Sen, S. K. St. Angelo, Y. Cao, T. E. Mallouk, P. E. Lammert, and V. H. Crespi, "Catalytic nanomotors: autonomous movement of striped nanorods," *Journal of the American Chemical Society*, vol. 126, no. 41, pp. 13424-13431, September 2004.

[11] S. Fournier-Bidoz, A. C. Arsenault, I. Manners, and G. A. Ozin, "Synthetic self-propelled nanorotors," *Chemical Communication*, vol. 441, pp. 441-443, November 2004.

[12] J. R. Howse, J. R. Howse, A. J. Ryan, T. Gough, R. Vafabakhsh, and R. Golestanian, "Self-Motile colloidal particles: from directed propulsion to random walk," *Physical Review Letters*, vol. 99, no. 4, 048102, July 2007.

[13] R. Dreyfus1, J. Baudry, M. L. Roper, M. Fermigier, H. A. Stone, J. Bibette, "Microscopic artificial swimmers,", *Nature*, vol. 437, October 2005.

[14] M. P. Kummer, J. J. Abbott, B. E. Kartochvil, R. Borer, A. Sengul, and B. J. Nelson, "OctoMag: an electromagnetic system for 5-DOF wireless micromanipulation," *IEEE Transactions on Robotics*, vol. 26, no. 6, pp. 1006-1017, December 2010.

[15] B. E. Kratochvil, M. P. Kummer, S. Erni, R. Borer, D. R. Frutiger, S. Schurle, and B. J. Nelson, "MiniMag: a hemispherical electromagnetic system for 5-DOF wireless micromanipulation," *Proceeding of the 12th International Symposium on Experimental Robotics*, New Delhi, India, December 2010.

[16] J. J. Abbott, O. Ergeneman, M. P. Kummer, A. M. Hirt, and B. J. Nelson, "Modeling magnetic torque and force for controlled manipulation of soft-magnetic bodies," *IEEE Transactions on Robotics and Automation*, vol. 23, no. 6, pp. 1247-1252, December 2007.

[17] K. E. Peyer, L. Zhang, B. J. Nelson, "Bio-inspired magnetic swimming microrobots for biomedical application," *Nanoscale*, vol. 5, no. 4, pp. 1259-1272, November 2012.

[18] D. J. Bell, S. Leutenegger, K. M. Hammar, L. X. Dong, B. J. Nelson, "Flagella-like propulsion for microrobots using a magnetic nanocoil and a rotating electromagnetic field," in *Proceedings of the IEEE International Conference on Robotics and Automation (ICRA)*, pp. 1128-1133, April 2007.

[19] A. W. Mahoney, D. L. Cowan, K. M. Miller, and J. J. Abbott, "Control of untethered magnetically actuated tools using a rotating permanent magnet in any position," in *Proceedings of the IEEE International Conference on Robotics and Automation (ICRA)*, pp. 3375-3380, Minnesota, USA, May 2012.

[20] A. W. Mahoney and J. J. Abbott, "Control of untethered magnetically actuated tools with localization uncertainty using a rotating permanent magnet," in *Proceedings of the IEEE RAS/EMBS International Conference on Biomedical Robotics and Biomechatronics (BioRob)*, pp. 1632-1637, Rome, Italy, June 2012.

[21] G. Kósa, P. Jakab, N. Hata, F. Jlesz, Z. Neubach, M. Shoham, M. Zaaroor and G. Szkely, "Flagellar Swimming for Medical Micro Robots: Theory, Experiments and Application," in *Proceedings of the IEEE RAS/EMBS International Conference on Biomedical Robotics and Biomechatronics (BioRob)*, pp. 258-263, October 2008.

[22] Z. Ye, S. Régnier, and M. Sitti,, "Rotating magnetic miniature swimming robots with multiple flexible flagella," *IEEE Transactions on Robotics and Automation*, vol. 30, no. 1, pp. 3-13, February 2014.

[23] T. H. Boyer, "The force on a magnetic dipole," *American Journal of Physics*, vol. 56, no. 8, pp. 688-692, August 1988.

[24] S. S. Shevkoplyas, A. C. Siegel, R. M. Westervelt, M. G. Prentiss, and G. M. Whitesides, "The force acting on a superparamagnetic bead due to an applied magnetic field," *Lab on a Chip*, vol. 7, no. 6, pp. 1294-1302, July 2007.

[25] T. J. Ui, R. G. Hussey, and R. P. Roger, "Stokes drag on a cylinder in axial motion," *Physics of Fluids*, vol. 27, no. 787, pp. 787-795, April 1984.

[26] I. S. M. Khalil, V. Magdanz, S. Sanchez, O. G. Schmidt, and S. Misra, "Three-dimensional closed-loop control of self-propelled microjets," *Applied Physics Letters*, 103, 172404, October 2013.

[27] I. S. M. Khalil, P. Ferreira, R. Eleutério, C. L. de Korte, and S. Misra, "Magnetic-Based closed-loop control of paramagnetic microparticles using ultrasound feedback," in *Proceedings of the IEEE International Conference on Robotics and Automation (ICRA)*, pp. 3807-3812, Hong Kong, China, June 2014.

[28] I. S. M. Khalil, L. Abelmann, and S. Misra, "Magnetic-Based motion control of paramagnetic microparticles with disturbance compensation," *IEEE Transactions on Magnetics*, May 2014. *In Press*